



1     **A new steady-state gas/particle partitioning model of PAHs: Implication for the**  
2                                   **influence of the particulate proportion in emissions**

3     Fu-Jie Zhu<sup>a,b</sup>, Peng-Tuan Hu<sup>a,c</sup>, Wan-Li Ma<sup>a,b,\*</sup>

4     <sup>a</sup> International Joint Research Center for Persistent Toxic Substances (IJRC-PTS), State  
5     Key Laboratory of Urban Water Resource and Environment, Harbin Institute of  
6     Technology, Harbin 150090, China

7     <sup>b</sup> Heilongjiang Provincial Key Laboratory of Polar Environment and Ecosystem  
8     (HPKL-PEE), Harbin 150090, China

9     <sup>c</sup> School of Environment, Key Laboratory for Yellow River and Huai River Water  
10    Environment and Pollution Control, Ministry of Education, Henan Normal University,  
11    Xinxiang, China

12

---

\*Corresponding author. International Joint Research Center for Persistent Toxic Substances (IJRC-PTS), State Key Laboratory of Urban Water Resource and Environment, Harbin Institute of Technology, 73 Huanghe Road, Nangang District, Harbin 150090, Heilongjiang, China.

Email address: [mawanli002@163.com](mailto:mawanli002@163.com)



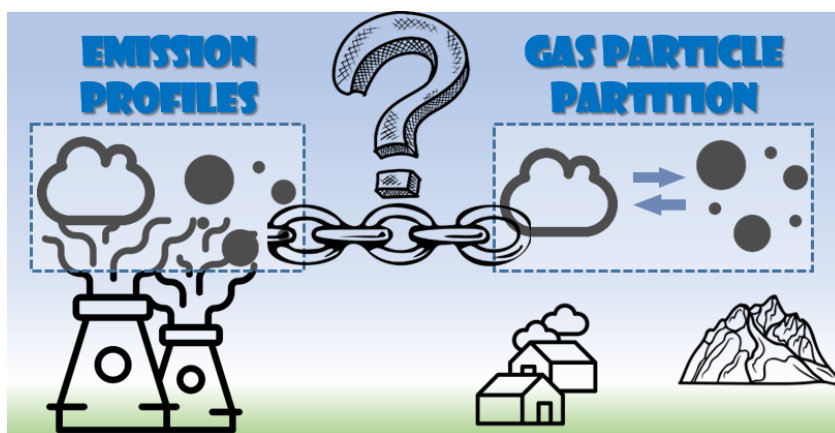
13 **Abstract:**

14 Gas/particle (G/P) partitioning is an important atmospheric process for semi-volatile  
15 organic compounds (SVOCs). However, the exact prediction of the G/P partitioning  
16 coefficients ( $K_P$ ) of polycyclic aromatic hydrocarbons (PAHs) was still a challenge. In  
17 this study, a new steady-state G/P partitioning model was established based on the level  
18 III multimedia fugacity model, with the introduction of the particulate proportion of  
19 PAHs in emission ( $\phi_0$ ) particularly. Same with the previous steady-state model, three  
20 different domains with different G/P partitioning behavior can be divided by the  
21 threshold values of  $\log K_{OA}$  (octanol-air partitioning coefficient). The difference  
22 between the new steady-state model and previous G/P partitioning models was quite  
23 different in different domains. It was found that the deviation with the  $K_P$  of PAHs from  
24 the equilibrium state was caused by both the gaseous and particulate interferences, in  
25 which  $\phi_0$  determined the influence of the two interferences. Different forms of the new  
26 steady-state model were observed under different values of  $\phi_0$ . The comparison with  
27  $\log K_P$  of PAHs between the prediction result of the new steady-state model and the  
28 monitored results from 11 cities in China indicated that the  $\phi_0$  was an important factor  
29 for the G/P partitioning of PAHs. In addition, the new steady-state model also showed  
30 good performance for the prediction of  $\log K_P$  of PAHs with totally gaseous emission  
31 and PBDEs with totally particulate emission. Therefore, it can be concluded that the  $\phi_0$   
32 should be considered in the study of G/P partitioning of PAHs, which also provided a  
33 new insight for other SVOCs.

34



35 Graphical Abstracts



36



37 **1. Introduction**

38 Atmospheric long-range transport can move the semi-volatile organic compounds  
39 (SVOCs) from sources to remote regions, such as the Arctic and the Tibetan Plateau,  
40 where the SVOCs are not produced and used (Hung et al., 2005; Hung et al., 2010;  
41 Wang et al., 2018a). The gas/particle (G/P) partitioning of SVOCs is an important  
42 atmospheric process, which governs their long-range transport and fate in atmosphere  
43 (Zhao et al., 2020; Li et al., 2015). For example, the wet and dry depositions of SVOCs  
44 are controlled by the distribution between gas phase and particle phase, thus affecting  
45 the efficiency and scope of long-range transport from sources to remote regions  
46 (Bidleman, 1988). In addition, the routes of entering the human body are also different  
47 for gaseous and particulate SVOCs, which indicated that the G/P partitioning of SVOCs  
48 is also a significant issue for human exposure assessment (Weschler et al., 2015; Hu et  
49 al., 2021).

50 The G/P partitioning of SVOCs has been studied for decades, and some models  
51 were developed for the prediction of the G/P partitioning coefficient ( $K_p$ ) of SVOCs  
52 (Zhu et al., 2021; Qiao et al., 2020a). Recently, Qiao et al. (2020a) summarized eight  
53 G/P partitioning models into three groups: (1) the models based on the equilibrium-  
54 state theory (Pankow, 1987; Harner and Bidleman, 1998; Dachs and Eisenreich, 2000;  
55 Goss, 2005; Shahpoury et al., 2016), (2) the empirical models based on monitoring data  
56 (Li and Jia, 2014; Wei et al., 2017), and (3) the models based on the steady-state theory  
57 (Li et al., 2015). In addition, a new empirical model (equation) for polycyclic aromatic  
58 hydrocarbons (PAHs) (Zhu et al., 2022) and a new steady-state mass balance model for  
59 polybrominated diphenyl ethers (PBDEs) (Zhao et al., 2020) have been established  
60 recently for the prediction of  $K_p$ . In general, the effectiveness and performance of these  
61 models have been evaluated with field monitoring programs (Vuong et al., 2020; Qiao



62 et al., 2019), and these models have been frequently used for predicting the G/P  
63 partitioning behavior of SVOCs (Qiao et al., 2020b).

64 Along with the concurrent formation of particle, the G/P partitioning process of  
65 PAHs was more complex than other SVOCs (Dachs and Eisenreich, 2000; Shahpoury  
66 et al., 2016; Zhu et al., 2021). For example, it was found that when the value of octanol-  
67 air partitioning coefficient ( $\log K_{OA}$ ) was more than 12, the monitored values of  $K_P$  of  
68 PAHs varied from both the predictions of the equilibrium-state G/P partitioning models  
69 and the steady-state G/P partitioning models (Ma et al., 2020; Zhu et al., 2021). Recent  
70 studies have found that the particulate proportion of SVOCs in the emissions ( $\phi_0$ ) could  
71 affect the G/P partitioning of SVOCs (Qin et al., 2021; Zhao et al., 2020). For example,  
72 when  $\phi_0$  increased, the predictions could diverge from the steady-state G/P partitioning  
73 model to the equilibrium-state G/P partitioning model (Qin et al., 2021; Zhao et al.,  
74 2020). Furthermore, the emission sources of PAHs in atmosphere are complex,  
75 including stationary sources (residential combustion, industrial production and  
76 agricultural burning) and mobile sources (motor vehicles, railways, and shipping)  
77 (Zhang et al., 2020; Tang et al., 2020), in which the gaseous and particulate PAHs both  
78 exist (Zimmerman et al., 2019; Wang et al., 2018b; Shen et al., 2011; Cai et al., 2018b).  
79 Therefore, the detailed influence of  $\phi_0$  on the G/P partitioning of PAHs might be  
80 considered for the deviation of the measured  $K_P$  from both the equilibrium-state G/P  
81 partitioning model and the steady-state G/P partitioning model predictions.

82 In this study, a new steady-state G/P partitioning model (called the new steady-  
83 state model for short hereafter) was established based on the level III multimedia  
84 fugacity model for PAHs, and the influence of  $\phi_0$  of PAHs in emissions was  
85 comprehensively discussed. The following topics were conducted: (1) the new steady-  
86 state model was established and deeply studied under different threshold values of log

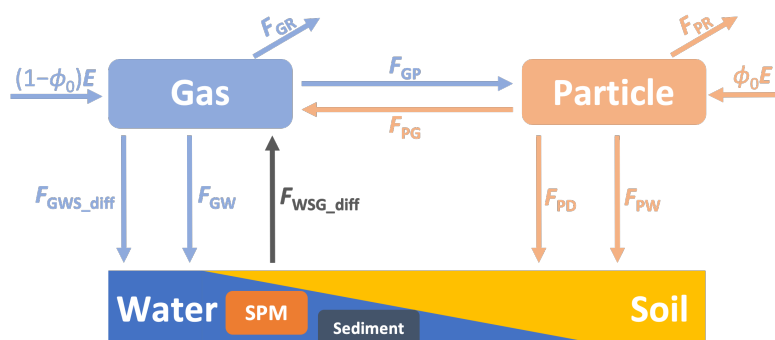


87  $K_{OA}$ ; (2) the influence of  $\phi_0$  on the G/P partitioning of PAHs was comprehensively  
 88 discussed; and (3) the performance of the new steady-state model for the prediction of  
 89  $K_P$  of PAHs were discussed finally.

90 **2. Establishment of the new steady-state G/P partitioning model**

91 **2.1. Establishment method of the new steady-state model**

92 A steady-state six-compartment six-fugacity model was applied in the present  
 93 study, which can be found in detail in **Text S1, Supporting Information (SI)**. The  
 94 input and output fluxes of gas phase and particle phase PAHs were presented in **Fig. 1**.  
 95 The detailed calculation methods for these fluxes can be found in **Text S2, SI**.



96

97 Fig. 1. The fluxes related to the gas and particle phase in the six-compartment model

98 (Note:  $F_{GR}$ : degradation flux of gas phase PAHs;  $F_{PR}$ : degradation flux of particle phase PAHs;

99  $F_{GP}$ : migration flux from gas phase to particle phase;  $F_{PG}$ : migration flux from particle phase to

100 gas phase;  $F_{GWS\_diff}$ : diffusion fluxes from gas phase to water and/or soil phases;  $F_{GW}$ : wet

101 deposition flux of gas phase PAHs to water and/or soil phase;  $F_{WSG\_diff}$ : diffusion fluxes from soil

102 and/or water phases to gas phase;  $F_{PD}$ : dry deposition flux of particle phase PAHs to SPM and/or

103 soil phase;  $F_{PW}$ : wet deposition flux of particle phase PAHs to SPM and/or soil phase;  $(1-\phi_0)E$ :

104 emission flux of gas phase PAHs;  $\phi_0 E$ : emission flux of particle phase PAHs.)

105 The input and output fluxes of gas phase and particle phase were compared in four

106 groups (input fluxes of gas phase, output fluxes of gas phase, input fluxes of particle



107 phase, and output fluxes of particle phase), and the results for PAHs were presented in  
 108 **Fig. S1, SI**. It can be found that the four fluxes ( $F_{GWS\_diff}$ ,  $F_{WSG\_diff}$ ,  $F_{PR}$ , and  $F_{GW}$ ) can  
 109 be removed from the system due to their ignored proportion in each group. After  
 110 simplifying the function in **Text S1, SI**, the two linear equations describing the input  
 111 and output fluxes of gas phase and particle phase can be established as follows:

$$112 \quad \begin{cases} (1 - \phi_0)E + D_{GP}f_P = (D_{GR} + D_{GP})f_G \\ \phi_0E + D_{GP}f_G = (D_{GP} + D_{PD} + D_{PW})f_P \end{cases} \quad (1)$$

113 where,  $f_P$  is the fugacity for particle phase;  $f_G$  is the fugacity for gas phase;  $D_{GP}$  is the  
 114 intermedia  $D$  value between gas phase and particle phase;  $D_{GR}$  is the  $D$  value for the  
 115 degradation of gas phase PAHs;  $D_{PD}$  and  $D_{PW}$  are the  $D$  values of the dry and wet  
 116 depositions of particle phase PAHs, respectively.

117 The fugacity ratio of the particle phase to the gas phase can be obtained by solving  
 118 the Eq. (1) as follows:

$$119 \quad \frac{f_P}{f_G} = \frac{D_{GP} + \phi_0 D_{GR}}{D_{GP} + (1 - \phi_0)(D_{PD} + D_{PW})} \quad (2)$$

120 According to the calculation of log  $K_P$  from the fugacity method (Li et al., 2015)  
 121 (See details in **Text S3, SI**), the new steady-state model can be expressed as follows:

$$122 \quad \log K_{P-NS} = \log K_{P-HB} + \log\left(\frac{D_{GP} + \phi_0 D_{GR}}{D_{GP} + (1 - \phi_0)(D_{PD} + D_{PW})}\right) \quad (3)$$

123 In the Eq. (3), the log  $K_{P-HB}$  is the equilibrium-state G/P partitioning model (named  
 124 as the H-B model in this study,  $\log K_{P-HB} = \log K_{OA} + \log f_{OM} - 11.91$ , and  $f_{OM}$  is the  
 125 fraction of organic matters in particles) (Harner and Bidleman, 1998). The part of  $D_{GR}$ ,  
 126 caused by the degradation of PAHs in gas phase, is defined as the gaseous interference,  
 127 and the part of  $D_{PD} + D_{PW}$ , caused by the deposition of PAHs in particle phase, is  
 128 defined as the particulate interference. Therefore, the levels of the influences of the two  
 129 interferences were based on the value of  $\phi_0$ .



130 By applying the calculation method of the  $D$  values in the multimedia fugacity  
131 model (**Table S1, SI**) and the values of the related parameters in the **Tables S2, S3, S4,**  
132 **S5, and S6, SI**, the Eq. (2) can be simplified as follows:

$$133 \quad \frac{f_P}{f_G} = \frac{1+13.2\phi_0 \times k_{deg}}{1+10^{-10.31}(1-\phi_0)f_{OM}K_{OA}} \quad (4)$$

134 where,  $k_{deg}$  is the degradation rate of PAHs in gas phase ( $h^{-1}$ ); and  $K_{OA}$  is the octanol-  
135 gas partitioning coefficient.

136 Therefore, the Eq. (3) can be also expressed as follows:

$$137 \quad \log K_{P-NS} = \log K_{P-HB} + \log\left(\frac{1+13.2\phi_0 \times k_{deg}}{1+10^{-10.31}(1-\phi_0)f_{OM}K_{OA}}\right) \quad (5)$$

138 Thus, it can be found that the new steady-state model ( $\log K_{P-NS}$ ) is a function of  
139  $\phi_0$ ,  $k_{deg}$ ,  $f_{OM}$  and  $K_{OA}$ .

## 140 2.2. Different domains of the new steady-state model

141 Three domains were identified according to the threshold values of  $\log K_{OA}$ . For  
142 example, if  $10^{-10.31}(1-\phi_0)f_{OM}K_{OA} \ll 1$ , the first threshold of  $\log K_{OA}$  ( $\log K_{OA1}$ ) can  
143 be obtained. Then, the Eq. (5) is expressed as follows:

$$144 \quad \log K_{P-NS} = \log K_{P-HB} + \log(1 + 13.2\phi_0 \times k_{deg}) \quad (6)$$

145 In this domain, the value of  $\log K_{OA}$  was less than  $\log K_{OA1}$ , and the  $\log K_{P-NS}$  was  
146 related to  $K_{OA}$ ,  $f_{OM}$ ,  $\phi_0$  and  $k_{deg}$ . The domain was presented with vertical lines as  
147 background in **Fig. 2**.

148 In addition, if  $10^{-10.31}(1-\phi_0)f_{OM}K_{OA} \gg 1$ , the second threshold of  $\log K_{OA}$  ( $\log$   
149  $K_{OA2}$ ) can be obtained. The Eq. (5) is expressed as follows:

$$150 \quad \log K_{P-NS} = \log K_{P-HB} + \log\left(\frac{1+13.2\phi_0 \times k_{deg}}{10^{-10.31}(1-\phi_0)f_{OM}K_{OA}}\right) \quad (7)$$

151 By substituting the  $\log K_{P-HB}$  using the equation ( $\log K_{P-HB} = \log K_{OA} + \log f_{OM}$   
152  $-11.91$ ) (Harner and Bidleman, 1998), the Eq. (7) can be simplified as follows:





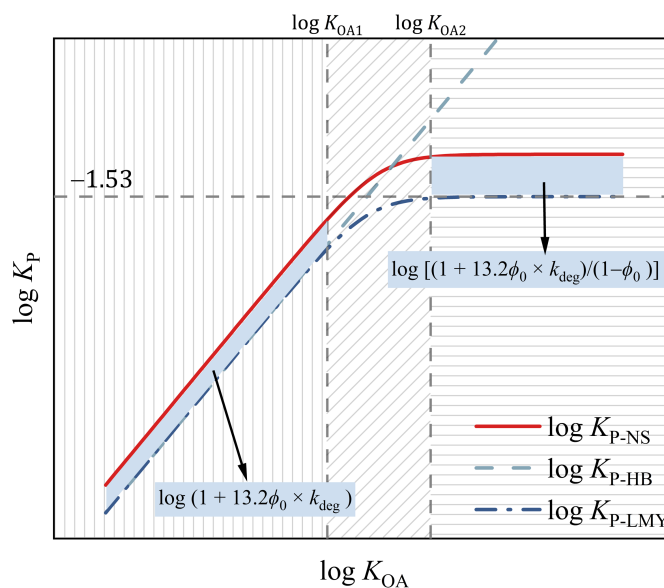
153 
$$\log K_{P-NS} = \log \left( \frac{1+13.2\phi_0 \times k_{deg}}{1-\phi_0} \right) - 1.6 \quad (8)$$

154 In this domain, the value of  $\log K_{OA}$  was higher than  $\log K_{OA2}$ , the  $\log K_{P-NS}$  was  
155 only related to  $\phi_0$  and  $k_{deg}$ , and the  $\log K_{P-NS}$  will be a maximum constant ( $\log K_{P-NSmax}$ ),  
156 as the part with horizontal lines as background in **Fig. 2**.

157 Furthermore, when  $\log K_{OA1} < \log K_{OA} < \log K_{OA2}$ , the  $\log K_{P-NS}$  increased along  
158 with the increasing of  $\log K_{OA}$ , and the increasing rate (or the slope of the function of  
159  $\log K_{P-NS}$  (Eq. 5)) decreased from 1 to 0. The  $\log K_{P-NS}$  was related to  $K_{OA}$ ,  $f_{OM}$ ,  $\phi_0$  and  
160  $k_{deg}$ . This domain was presented as the part in with diagonal lines as background **Fig. 2**.

### 161 **2.3. Difference between of the new steady-state model and other previous models**

162 The difference between the new steady-state model with the H-B model (**Text S4**,  
163 **SI**) and the L-M-Y model (the steady-state model) (Li et al., 2015) (**Text S4**, **SI**) can  
164 be calculated by the Eq. (5) in different domains. Briefly, as shown in **Fig. 2**, when  $\log$   
165  $K_{OA} < \log K_{OA1}$ , the difference between the new steady-state model and the H-B model  
166 or the L-M-Y model can be expressed as  $\delta_1 = \log (1 + 13.2\phi_0 \times k_{deg})$ . The value of  $\delta_1$   
167 increased along with the increase of  $\phi_0$ , and will reach the maximum value of  $\log (1 +$   
168  $13.2k_{deg})$  when  $\phi_0 = 1$  (**Fig. S2a**, **SI**). When  $\log K_{OA} > \log K_{OA2}$ , the difference between  
169 the new steady-state model and the L-M-Y model can be expressed as  $\delta_2 = \log [(1 +$   
170  $13.2\phi_0 \times k_{deg}) / (1 - \phi_0)]$ . The value of  $\delta_2$  also increased along with the increase of  $\phi_0$ ,  
171 and will approach infinity when  $\phi_0$  infinitely close to 1 (**Fig. S2b**, **SI**). When  $\log K_{OA1}$   
172  $< \log K_{OA} < \log K_{OA2}$ , the difference between the new steady-state model and the L-M-  
173 Y model was the function of  $\phi_0$  and  $K_{OA}$ , which increased along with the increasing of  
174  $\phi_0$  and  $K_{OA}$ , and more detailed information can be found in next section.



175

176 Fig. 2. The three domains of the new steady-state G/P partitioning model divided by the two  
 177 threshold values of  $\log K_{OA}$

178 **3. Influence of  $\phi_0$  on  $K_P$  of PAHs**

179 In general, the different values of  $\phi_0$  are corresponding to different forms of the  
 180 new steady-state model (Eq. (3)). Three different forms can be obtained under different  
 181 values of  $\phi_0$  ( $0 < \phi_0 < 1$ ,  $\phi_0 = 0$ , and  $\phi_0 = 1$ ).

182 When  $0 < \phi_0 < 1$ , the particle phase and gas phase PAHs both exist in the emission,  
 183 and the new steady-state model is expressed as Eq. (3). In this form, the gaseous  
 184 interference and the particulate interference all need to be considered for the G/P  
 185 partitioning of PAHs in atmosphere. The deviation of the new steady-state model from  
 186 the H-B model, depends on the ratio of  $\phi_0 D_{GR}$  to  $(1 - \phi_0)(D_{PD} + D_{PW})$ . When the ratio  
 187 was higher than 1, the  $\log K_{P-NS}$  presented upwards from the prediction of the H-B  
 188 model, while the  $\log K_{P-NS}$  presented downwards, when the ratio was lower than 1.

189 When  $\phi_0 = 0$ , the PAHs in the emission is totally gaseous PAHs, and the Eq. (3) is  
 190 expressed as follows:



191 
$$\log K_{P-NS} = \log K_{P-HB} + \log\left(\frac{D_{GP}}{D_{GP} + (D_{PD} + D_{PW})}\right) \quad (10)$$

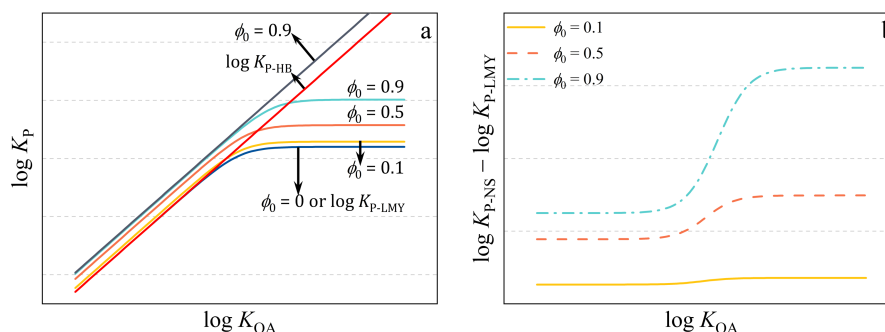
192 In fact, this equation is identical to that of the L-M-Y model, where  $\alpha = D_{GP} / (D_{GP}$   
193  $+ D_{PD} + D_{PW})$  (Li et al., 2015).

194 When  $\phi_0 = 1$ , the PAHs in the emission is totally particulate PAHs, and the Eq. (3)  
195 is expressed as follows:

196 
$$\log K_{P-NS} = \log K_{P-HB} + \log\left(\frac{D_{GP} + D_{GR}}{D_{GP}}\right) \quad (11)$$

197 The derivation of the new steady-state model from the H-B model was mainly  
198 caused by the degradation of PAHs in gas phase. When  $k_{deg}$  is small enough to be  
199 ignored, the new steady-state model is equal to the H-B model.

200 The specific influence of  $\phi_0$  on  $K_P$  of PAHs was studied with different values of  
201  $\phi_0$ , and the results are showed in **Fig. 3**. As exhibited in **Fig. 3a**, the prediction line of  
202 the new steady-state model diverged from the L-M-Y model to the H-B model with the  
203 increasing of  $\phi_0$ , which was consistent with the results reported in previous studies  
204 (Zhao et al., 2020; Qin et al., 2021). In addition, obvious differences were observed  
205 between the prediction lines for the three models. In particular, when  $\phi_0 = 1$ , the line of  
206  $\log K_{P-NS}$  was parallel with the line of  $\log K_{P-HB}$ . When  $\phi_0 = 0$ , the prediction line of  $\log$   
207  $K_{P-NS}$  was same with that of  $\log K_{P-LMY}$ . When  $0 < \phi_0 < 1$ , the trends of the prediction  
208 lines of  $\log K_{P-NS}$  were similar to that of  $\log K_{P-LMY}$ . The deviations between the  
209 prediction lines of  $\log K_{P-NS}$  and  $\log K_{P-LMY}$  are showed in **Fig. 3b**. In general, the  
210 deviations between the prediction lines varied with the values of  $\phi_0$  and  $\log K_{OA}$ . In  
211 addition, the deviation became larger along with the increase of  $\phi_0$ . And the deviation  
212 exhibited three different trends along with the increasing of  $\log K_{OA}$  separated by the  
213 two threshold values of  $\log K_{OA}$  ( $\log K_{OA1}$  and  $\log K_{OA2}$ ).



214

215 Fig. 3. The comparison between the new steady-state model and the H-B model and the L-M-Y  
 216 model (Note: a, the prediction lines of the three models; b, the difference between the new steady-  
 217 state model and the L-M-Y model with different values of  $\phi_0$ .)

#### 218 4. Validation of the new steady-state G/P partitioning model

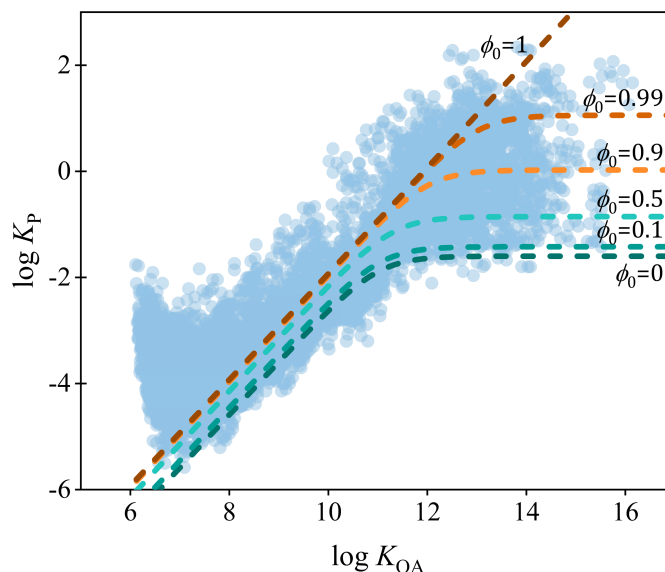
##### 219 4.1. Validation

220 As we know, the emission sources of PAHs in atmosphere is complex, including  
 221 stationary sources and mobile sources (Zhang et al., 2020). Furthermore, various  
 222 proportions of particulate PAHs were also reported in different emission sources  
 223 (Zimmerman et al., 2019; Wang et al., 2018b; Shen et al., 2011; Cai et al., 2018b).  
 224 Therefore, the precise values of  $\phi_0$  cannot be easily confirmed. In this section, the  
 225 different values of  $\phi_0$  (0, 0.1, 0.5, 0.9, 0.99, and 1) were considered with the new steady-  
 226 state model for the prediction of  $K_P$  of PAHs in order to obtain representative results.

227 In order to evaluate the performance of the new steady-state model, the monitored  
 228 values of the  $\log K_P$  of PAHs from 11 cities across China were applied (Ma et al., 2018;  
 229 Ma et al., 2019; Ma et al., 2020). As showed in Fig. 4, the prediction line of the new  
 230 steady-state model matched well with the monitoring data of  $\log K_P$ . Especially for the  
 231 monitoring data with high  $\log K_{OA}$ , the data mainly distributed between the prediction  
 232 lines of the steady-state model with the values of  $\phi_0$  from 0 to 1. In addition, for different  
 233 cities (Fig. S3, SI), the values of  $\phi_0$  for the best matched prediction lines of the new



234 steady-state model were different, which was expected since the sources of PAHs were  
235 also different among the 11 cities. The matching degree of the new steady-state model  
236 was also evaluated by the method of the root mean square error (*RMSE*, **Text S5, SI**).  
237 In general, for PAHs with higher values of  $\log K_{OA}$  (such as the high molecular weight  
238 PAHs), when  $\phi_0$  were 0.9 or 0.99, the value of *RMSE* for each city was the lowest (**Fig.**  
239 **S4, SI**), which indicated the best matching degree between the prediction results and  
240 the monitoring results. Actually, previous studies found that high molecular weight  
241 PAHs were dominant in particle phase in emissions with higher  $\phi_0$  (Shen et al., 2011;  
242 Mastral et al., 1996; Lu et al., 2009), which indicated that our findings were reasonable.



243

244 Fig. 4. The comparison between the monitored data of  $\log K_P$  of PAHs from 11 cities in China and  
245 the prediction lines of the new steady-state model with different values of  $\phi_0$

246 Furthermore, the performance of the new steady-state model for the prediction of  
247  $\log K_P$  of PAHs in special scenario was also discussed. It was found that in the prototype  
248 coking plant, the removal efficiency of dust was 96% (Liu et al., 2019). In this scenario,  
249 the gaseous PAHs dominated in the emission, and the values of  $\phi_0$  can be considered as



250  $\sim 0$ . As showed in **Fig. S5, SI**, the monitored data of  $\log K_P$  from the coking plant  
251 matched best with the prediction line of the new steady-state model with  $\phi_0 = 0$ , with  
252 the lowest *RMSE*. According to the comparison, the best matched  $\phi_0$  in the steady-state  
253 model was consistent with that in the emission profile. The results indicated the good  
254 performance of the new steady-state model in this special scenario.

255 Furthermore, although the model was developed based on the parameters of PAHs,  
256 taking into account comparable partitioning characteristics of SVOCs, the steady-state  
257 model could be expanded to other SVOCs. A special scenario with the recycling of  
258 electrical and electronic waste site (E-waste site) was considered to validate the  
259 performance of the new steady-state model for other SVOCs. In this case, PBDEs were  
260 mainly in particle phase in the emissions, and the values of  $\phi_0$  can be considered as  $\sim 1$   
261 (Cai et al., 2018a). **Fig. S6, SI** illustrates the comparison between the monitored data  
262 of  $\log K_P$  from several E-waste sites (Tian et al., 2011; Han et al., 2009; Chen et al.,  
263 2011) and the prediction lines of the new steady-state model with different values of  $\phi_0$   
264 (0, 0.1, 0.5, 0.9, 0.99, and 1). The related results for *RMSE* are showed in **Fig. S7, SI**.  
265 It is interesting to note that the monitored data of  $\log K_P$  matched best with the  
266 prediction line of the new steady-state model with  $\phi_0 = 1$ , which also had the lowest  
267 values of *RMSE*. Therefore, it can be concluded that the new steady-state model could  
268 be expanded to the prediction of  $K_P$  of PBDEs in E-waste sites.

#### 269 **4.2. Implication**

270 The present study has established a new steady-state G/P partitioning model,  
271 which takes into account the particulate proportion of SVOCs in emission. In summary,  
272 the study provided a new insight for the field of G/P partitioning and other related fields  
273 with SVOCs. Firstly, if the SVOCs in atmosphere are from diverse sources of emissions  
274 with different  $\phi_0$ , the new steady-state model is much more suitable for the G/P



275 partitioning study and related studies, such as health risk assessment. Secondly, when  
276 studying the pollution characteristic and regional transport of SVOCs from a single  
277 point source, such as the transport of PBDEs around an E-waste site or the transport of  
278 SVOCs around chemical factories, the G/P partitioning of SVOCs must take into  
279 account the particulate proportion of SVOCs in emissions. Thirdly, for long-range  
280 atmospheric transport studies, if there are various sources of SVOCs along the transport  
281 route, the continuous effect of the particulate proportion of SVOCs in emissions on the  
282 transport and fate of SVOCs requires careful consideration, such as the establishment  
283 of atmospheric transport model.

#### 284 **4.3. Limitation**

285 Based on the above discussion, it can be concluded that the new steady-state model  
286 had good performance for the prediction of  $K_P$  of PAHs in various real atmospheres,  
287 which provided a new method for the studying on the G/P partitioning of PAHs.  
288 However, some limitations of the new steady-state model still existed in the present  
289 study. First, the values of  $\phi_0$  were different between different compounds and different  
290 emission sources (Zimmerman et al., 2019; Wang et al., 2018b; Shen et al., 2011; Cai  
291 et al., 2018b). In this study, some constant values of  $\phi_0$  were used for the new steady-  
292 state model, which was only can be considered as special examples. The exact values  
293 of  $\phi_0$  should be used for the application of the new steady-state model in future. Second,  
294 for the gaseous degradation ( $k_{deg}$ ) and the fraction of the organic matter in particle ( $f_{OM}$ ),  
295 only one constant and common value was used for the new steady-state model. In  
296 general, these two parameters were also complicated in real atmosphere. For example,  
297 the  $k_{deg}$  was not only related to the physicochemical properties of chemicals, but also  
298 related to the environmental parameters, such as temperature and concentration (Wilson  
299 et al., 2020). In addition, even though the  $f_{OM}$  can be directly measured, the actual values



300 of  $f_{OM}$  also changed along with many factors, such as emission sources (Gaga and Ari,  
301 2019; Lohmann and Lammel, 2004) and particle sizes (Hu et al., 2020). Therefore, the  
302 exact values of  $\phi_0$ ,  $k_{deg}$  and  $f_{OM}$  for the real atmosphere should also be used for the  
303 application of the new steady-state model in future. Third, the new steady-state model  
304 was established based on a single multimedia environment, in which the advections of  
305 air and water were not considered. In addition, some fluxes were removed in order to  
306 simplify the parameters of the model. Therefore, the influence of all fluxes and  
307 parameters related to gas and particle compartments should be evaluated  
308 comprehensively in future. Furthermore, the validation and implication of the new  
309 steady-state G/P partitioning model should also be conducted for other SVOCs in real  
310 multimedia environment.

#### 311 **Author Contribution**

312 **Fu-Jie Zhu:** Methodology, Investigation, Writing - original draft preparation.

313 **Peng-Tuan Hu:** Writing - review & editing. **Wan-Li Ma:** Conceptualization,  
314 Methodology, Writing - review & editing.

#### 315 **Competing interests**

316 The authors declare that they have no conflict of interest.

#### 317 **Acknowledgments**

318 This study was supported by the National Natural Science Foundation of China (No.  
319 41671470 and No. 42077341). This study was partially supported by the State Key  
320 Laboratory of Urban Water Resource and Environment, Harbin Institute of Technology  
321 (No. 2020TS03) and the Heilongjiang Touyan Innovation Team Program, China.

322





323 **References**

- 324 Bidleman, T. F.: Atmospheric processes wet and dry deposition of organic compounds  
325 are controlled by their vapor-particle partitioning, *Environ. Sci. Technol.*, 22, 361-  
326 367, 10.1021/es00169a002, 1988.
- 327 Cai, C., Yu, S., Liu, Y., Tao, S., and Liu, W.: PBDE emission from E-wastes during  
328 the pyrolytic process: Emission factor, compositional profile, size distribution,  
329 and gas-particle partitioning, *Environ. Pollut.*, 235, 419-428,  
330 10.1016/j.envpol.2017.12.068, 2018a.
- 331 Cai, C., Yu, S., Li, X., Liu, Y., Tao, S., and Liu, W.: Emission characteristics of  
332 polycyclic aromatic hydrocarbons from pyrolytic processing during dismantling  
333 of electronic wastes, *J. Hazard. Mater.*, 351, 270-276,  
334 10.1016/j.jhazmat.2018.03.012, 2018b.
- 335 Chen, D., Bi, X., Liu, M., Huang, B., Sheng, G., and Fu, J.: Phase partitioning,  
336 concentration variation and risk assessment of polybrominated diphenyl ethers  
337 (PBDEs) in the atmosphere of an e-waste recycling site, *Chemosphere*, 82, 1246-  
338 1252, <https://doi.org/10.1016/j.chemosphere.2010.12.035>, 2011.
- 339 Dachs, J. and Eisenreich, S. J.: Adsorption onto aerosol soot carbon dominates gas-  
340 particle partitioning of polycyclic aromatic hydrocarbons, *Environ. Sci. Technol.*,  
341 34, 3690-3697, 10.1021/es991201+, 2000.
- 342 Gaga, E. O. and Ari, A.: Gas-particle partitioning and health risk estimation of  
343 polycyclic aromatic hydrocarbons (PAHs) at urban, suburban and tunnel  
344 atmospheres: Use of measured EC and OC in model calculations, *Atmospheric  
345 Pollution Research*, 10, 1-11, 10.1016/j.apr.2018.05.004, 2019.



- 346 Goss, K.-U.: Predicting the equilibrium partitioning of organic compounds using just  
347 one linear solvation energy relationship (LSER), *Fluid Phase Equilib.*, 233, 19-22,  
348 <https://doi.org/10.1016/j.fluid.2005.04.006>, 2005.
- 349 Han, W., Feng, J., Gu, Z., Chen, D., Wu, M., and Fu, J.: Polybrominated Diphenyl  
350 Ethers in the Atmosphere of Taizhou, a Major E-Waste Dismantling Area in China,  
351 *Bul. Environ. Contam. Toxicol.*, 83, 783-788, 10.1007/s00128-009-9855-9, 2009.
- 352 Harner, T. and Bidleman, T. F.: Octanol-air partition coefficient for describing  
353 particle/gas partitioning of aromatic compounds in urban air, *Environ. Sci.*  
354 *Technol.*, 32, 1494-1502, 1998.
- 355 Hu, P.-T., Ma, W.-L., Zhang, Z.-F., Liu, L.-Y., Song, W.-W., Cao, Z.-G., Macdonald,  
356 R. W., Nikolaev, A., Li, L., and Li, Y.-F.: Approach to Predicting the Size-  
357 Dependent Inhalation Intake of Particulate Novel Brominated Flame Retardants,  
358 *Environ. Sci. Technol.*, 55, 15236-15245, 10.1021/acs.est.1c03749, 2021.
- 359 Hu, P.-T., Su, P.-H., Ma, W.-L., Zhang, Z.-F., Liu, L.-Y., Song, W.-W., Qiao, L.-N.,  
360 Tian, C.-G., Macdonald, R. W., Nikolaev, A., Cao, Z.-G., and Li, Y.-F.: New  
361 equation to predict size-resolved gas-particle partitioning quotients for  
362 polybrominated diphenyl ethers, *J. Hazard. Mater.*, 400, 123245,  
363 <https://doi.org/10.1016/j.jhazmat.2020.123245>, 2020.
- 364 Hung, H., Blanchard, P., Halsall, C. J., Bidleman, T. F., Stern, G. A., Fellin, P., Muir,  
365 D. C. G., Barrie, L. A., Jantunen, L. M., Helm, P. A., Ma, J., and Konoplev, A.:  
366 Temporal and spatial variabilities of atmospheric polychlorinated biphenyls  
367 (PCBs), organochlorine (OC) pesticides and polycyclic aromatic hydrocarbons  
368 (PAHs) in the Canadian Arctic: Results from a decade of monitoring, *Science of*  
369 *the Total Environment*, 342, 119-144, 10.1016/j.scitotenv.2004.12.058, 2005.



- 370 Hung, H., Kallenborn, R., Breivik, K., Su, Y., Brorström-Lundén, E., Olafsdottir, K.,  
371 Thorlacius, J. M., Leppänen, S., Bossi, R., Skov, H., Manø, S., Patton, G. W.,  
372 Stern, G., Sverko, E., and Fellin, P.: Atmospheric monitoring of organic pollutants  
373 in the Arctic under the Arctic Monitoring and Assessment Programme (AMAP):  
374 1993–2006, *Science of the Total Environment*, 408, 2854-2873,  
375 <https://doi.org/10.1016/j.scitotenv.2009.10.044>, 2010.
- 376 Li, Y., Ma, W., and Yang, M.: Prediction of gas/particle partitioning of polybrominated  
377 diphenyl ethers (PBDEs) in global air: A theoretical study, *Atmospheric  
378 Chemistry and Physics*, 15, 1669-1681, 10.5194/acp-15-1669-2015, 2015.
- 379 Li, Y. F. and Jia, H. L.: Prediction of gas/particle partition quotients of Polybrominated  
380 Diphenyl Ethers (PBDEs) in north temperate zone air: An empirical approach,  
381 *Ecotoxicol. Environ. Saf.*, 108, 65-71, 2014.
- 382 Liu, X., Zhao, D., Peng, L., Bai, H., Zhang, D., and Mu, L.: Gas–particle partition and  
383 spatial characteristics of polycyclic aromatic hydrocarbons in ambient air of a  
384 prototype coking plant, *Atmos. Environ.*, 204, 32-42,  
385 <https://doi.org/10.1016/j.atmosenv.2019.02.012>, 2019.
- 386 Lohmann, R. and Lammel, G.: Adsorptive and absorptive contributions to the gas-  
387 particle partitioning of polycyclic aromatic hydrocarbons: State of knowledge and  
388 recommended parametrization for modeling, *Environ. Sci. Technol.*, 38, 3793-  
389 3803, 10.1021/es035337q, 2004.
- 390 Lu, H., Zhu, L., and Zhu, N.: Polycyclic aromatic hydrocarbon emission from straw  
391 burning and the influence of combustion parameters, *Atmos. Environ.*, 43, 978-  
392 983, <https://doi.org/10.1016/j.atmosenv.2008.10.022>, 2009.



- 393 Ma, W., Zhu, F., Hu, P., Qiao, L., and Li, Y.: Gas/particle partitioning of PAHs based  
394 on equilibrium-state model and steady-state model, *Sci. Total Environ.*, 706,  
395 136029, <https://doi.org/10.1016/j.scitotenv.2019.136029>, 2020.
- 396 Ma, W.-L., Zhu, F.-J., Liu, L.-Y., Jia, H.-L., Yang, M., and Li, Y.-F.: PAHs in Chinese  
397 atmosphere: Gas/particle partitioning, *Sci. Total Environ.*, 693, 133623,  
398 10.1016/j.scitotenv.2019.133623, 2019.
- 399 Ma, W. L., Liu, L. Y., Jia, H. L., Yang, M., and Li, Y. F.: PAHs in Chinese atmosphere  
400 Part I: Concentration, source and temperature dependence, *Atmos Environ*, 173,  
401 330-337, 2018.
- 402 Mastral, A. M., Callén, M., and Murillo, R.: Assessment of PAH emissions as a  
403 function of coal combustion variables, *Fuel*, 75, 1533-1536,  
404 [https://doi.org/10.1016/0016-2361\(96\)00120-2](https://doi.org/10.1016/0016-2361(96)00120-2), 1996.
- 405 Pankow, J. F.: Review and comparative analysis of the theories on partitioning between  
406 the gas and aerosol particulate phases in the atmosphere, *Atmos. Environ.*, 21,  
407 2275-2283, 1987.
- 408 Qiao, L., Hu, P., Macdonald, R., Kannan, K., Nikolaev, A., and Li, Y.-f.: Modeling  
409 gas/particle partitioning of polybrominated diphenyl ethers (PBDEs) in the  
410 atmosphere: A review, *Sci. Total Environ.*, 729, 138962,  
411 <https://doi.org/10.1016/j.scitotenv.2020.138962>, 2020a.
- 412 Qiao, L., Zhang, Z., Liu, L., Song, W., Ma, W., Zhu, N., and Li, Y.: Measurement and  
413 modeling the gas/particle partitioning of organochlorine pesticides (OCPs) in  
414 atmosphere at low temperatures, *Sci. Total Environ.*, 667, 318-324,  
415 10.1016/j.scitotenv.2019.02.347, 2019.
- 416 Qiao, L.-N., Hu, P.-T., Macdonald, R., Kannan, K., Nikolaev, A., and Li, Y.-F.:  
417 Modeling gas/particle partitioning of polybrominated diphenyl ethers (PBDEs) in



418 the atmosphere: A review, *Sci. Total Environ.*, 729, 138962,  
419 <https://doi.org/10.1016/j.scitotenv.2020.138962>, 2020b.

420 Qin, M., Yang, P., Hu, P., Hao, S., Macdonald, R. W., and Li, Y.: Particle/gas  
421 partitioning for semi-volatile organic compounds (SVOCs) in level III multimedia  
422 fugacity models: Both gaseous and particulate emissions, *Sci. Total Environ.*, 790,  
423 148012, <https://doi.org/10.1016/j.scitotenv.2021.148012>, 2021.

424 Shahpoury, P., Lammel, G., Albinet, A., Sofuoglu, A., Dumanoglu, Y., Sofuoglu, S.  
425 C., Wagner, Z., and Zdimal, V.: Evaluation of a conceptual model for gas-particle  
426 partitioning of polycyclic aromatic hydrocarbons using polyparameter linear free  
427 energy relationships, *Environ. Sci. Technol.*, 50, 12312-12319, 2016.

428 Shen, G., Wang, W., Yang, Y., Ding, J., Xue, M., Min, Y., Zhu, C., Shen, H., Li, W.,  
429 Wang, B., Wang, R., Wang, X., Tao, S., and Russell, A. G.: Emissions of PAHs  
430 from indoor crop residue burning in a typical rural stove: Emission factors, size  
431 distributions, and gas-particle partitioning, *Environ. Sci. Technol.*, 45, 1206-1212,  
432 10.1021/es102151w, 2011.

433 Tang, T., Cheng, Z., Xu, B., Zhang, B., Zhu, S., Cheng, H., Li, J., Chen, Y., and Zhang,  
434 G.: Triple Isotopes ( $\delta$  C-13,  $\delta$  H-2, and  $\delta$  C-4) Compositions and  
435 Source Apportionment of Atmospheric Naphthalene: A Key Surrogate of  
436 Intermediate-Volatility Organic Compounds (IVOCs), *Environ. Sci. Technol.*, 54,  
437 5409-5418, 10.1021/acs.est.0c00075, 2020.

438 Tian, M., Chen, S.-J., Wang, J., Zheng, X.-B., Luo, X.-J., and Mai, B.-X.: Brominated  
439 Flame Retardants in the Atmosphere of E-Waste and Rural Sites in Southern  
440 China: Seasonal Variation, Temperature Dependence, and Gas-Particle  
441 Partitioning, *Environ. Sci. Technol.*, 45, 8819-8825, 10.1021/es202284p, 2011.



- 442 Vuong, Q. T., Thang, P. Q., Nguyen, T. N. T., Ohura, T., and Choi, S. D.: Seasonal  
443 variation and gas/particle partitioning of atmospheric halogenated polycyclic  
444 aromatic hydrocarbons and the effects of meteorological conditions in Ulsan,  
445 South Korea, *Environ. Pollut.*, 263, 10.1016/j.envpol.2020.114592, 2020.
- 446 Wang, C., Wang, X., Gong, P., and Yao, T.: Long-term trends of atmospheric  
447 organochlorine pollutants and polycyclic aromatic hydrocarbons over the  
448 southeastern Tibetan Plateau, *Science of the Total Environment*, 624, 241-249,  
449 10.1016/j.scitotenv.2017.12.140, 2018a.
- 450 Wang, R., Liu, G., Sun, R., Yousaf, B., Wang, J., Liu, R., and Zhang, H.: Emission  
451 characteristics for gaseous- and size-segregated particulate PAHs in coal  
452 combustion flue gas from circulating fluidized bed (CFB) boiler, *Environ. Pollut.*,  
453 238, 581-589, 10.1016/j.envpol.2018.03.051, 2018b.
- 454 Wei, X., Yuan, Q., Serge, B., Xu, T., Ma, G., and Yu, H.: In silico investigation of  
455 gas/particle partitioning equilibrium of polybrominated diphenyl ethers (PBDEs),  
456 *Chemosphere*, 188, 110-118, <https://doi.org/10.1016/j.chemosphere.2017.08.146>,  
457 2017.
- 458 Weschler, C. J., Beko, G., Koch, H. M., Salthammer, T., Schripp, T., Toftum, J., and  
459 Clausen, G.: Transdermal Uptake of Diethyl Phthalate and Di(n-butyl) Phthalate  
460 Directly from Air: Experimental Verification, *Environ. Health Perspect.*, 123,  
461 928-934, 10.1289/ehp.1409151, 2015.
- 462 Wilson, J., Pöschl, U., Shiraiwa, M., and Berkemeier, T.: Non-equilibrium interplay  
463 between gas-particle partitioning and multiphase chemical reactions of semi-  
464 volatile compounds: mechanistic insights and practical implications for  
465 atmospheric modeling of PAHs, *Atmospheric Chemistry and Physics*, 2020, 1-39,  
466 10.5194/acp-2020-1000, 2020.



- 467 Zhang, L., Yang, L., Zhou, Q., Zhang, X., Xing, W., Wei, Y., Hu, M., Zhao, L., Toriba,  
468 A., Hayakawa, K., and Tang, N.: Size distribution of particulate polycyclic  
469 aromatic hydrocarbons in fresh combustion smoke and ambient air: A review,  
470 Journal of Environmental Sciences, 88, 370-384, 10.1016/j.jes.2019.09.007, 2020.
- 471 Zhao, F., Riipinen, I., and MacLeod, M.: Steady-state mass balance model for  
472 predicting particle–gas concentration ratios of PBDEs, Environ. Sci. Technol., 55,  
473 9425-9433, 10.1021/acs.est.0c04368, 2020.
- 474 Zhu, F.-J., Ma, W.-L., Zhang, Z.-F., Yang, P.-F., Hu, P.-T., Liu, L.-Y., and Song, W.-  
475 W.: Prediction of the gas/particle partitioning quotient of PAHs based on ambient  
476 temperature, Sci. Total Environ., 811, 151411,  
477 <https://doi.org/10.1016/j.scitotenv.2021.151411>, 2021.
- 478 Zhu, F.-J., Ma, W.-L., Zhang, Z.-F., Yang, P.-F., Hu, P.-T., Liu, L.-Y., and Song, W.-  
479 W.: Prediction of the gas/particle partitioning quotient of PAHs based on ambient  
480 temperature, Sci. Total Environ., 811, 151411,  
481 <https://doi.org/10.1016/j.scitotenv.2021.151411>, 2022.
- 482 Zimmerman, N., Rais, K., Jeong, C.-H., Pant, P., Mari Delgado-Saborit, J., Wallace, J.  
483 S., Evans, G. J., Brook, J. R., and Pollitt, K. J. G.: Carbonaceous aerosol sampling  
484 of gasoline direct injection engine exhaust with an integrated organic gas and  
485 particle sampler, Sci. Total Environ., 652, 1261-1269,  
486 10.1016/j.scitotenv.2018.10.332, 2019.
- 487